Article

Insights into PPARγ Phosphorylation and Its Inhibition Mechanism

Roberta Montanari,* Davide Capelli, Keiko Yamamoto, Hirono Awaishima, Kimina Nishikata, Arjan Barendregt, Albert J. R. Heck, Fulvio Loiodice, Fabio Altieri, Alessandro Paiardini, Alessandro Grottesi, Luciano Pirone, Emilia Pedone, Franck Peiretti, Jean Michel Brunel, Toshimasa Itoh,* and Giorgio Pochetti*
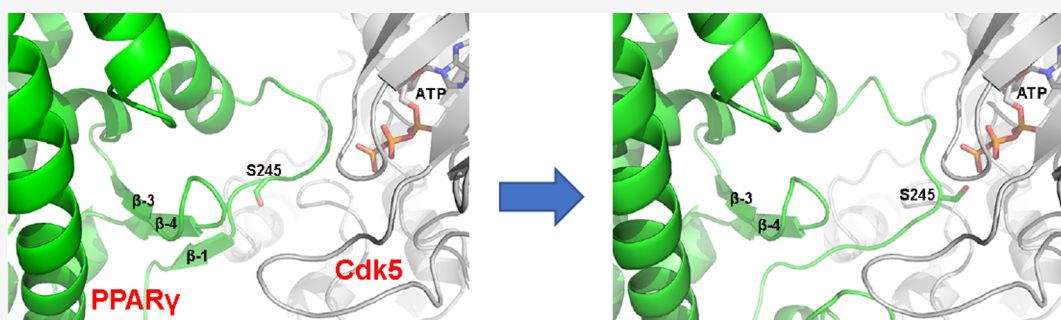
Read Online

ACCESS | Metrics & More | Article Recommendations | Supporting Information

ABSTRACT: PPARγ represents a key target for the treatment of type 2 diabetes and metabolic syndrome. Synthetic antidiabetic drugs activating PPARγ are accompanied by serious undesirable side effects related to their agonism. In the search for new PPARγ regulators, inhibitors of PPARγ phosphorylation on S245 mediated by CDK5 represent an opportunity for the development of an improved generation of antidiabetic drugs acting through this nuclear receptor. We have employed a multidisciplinary approach, including protein−protein docking, X-ray crystallography, NMR, HDX, MD simulations, and site-directed mutagenesis to investigate conformational changes in PPARγ that impair the ability of CDK5 to interact with PPARγ and hence inhibit PPARγ phosphorylation. Finally, we describe an alternative inhibition mechanism adopted by a ligand bound far from the phosphorylation site.

INTRODUCTION

The peroxisome proliferator-activated receptors (PPARs) are transcription factors that regulate glucose and lipid metabolism. The role of PPARs in several chronic diseases such as type 2 diabetes (T2D), obesity, and atherosclerosis is well-known.[1−3] Among the three subtypes (α, β/δ, and γ) PPARγ is the most widely studied as a therapeutically attractive target because of its key role in the regulation of energy balance and fat cell differentiation in the adipose tissue.[1,4−8] However, the initial clinical success of PPARγ agonists was soon overshadowed by several reports showing serious side effects,[9,10] linked to their agonism, which turned the enthusiasm into skepticism. In 2010, Choi and co-workers[11,12] described a new class of antidiabetic compounds devoid of side effects. The authors observed that phosphorylation of PPARγ by the cyclin-dependent kinase 5 (CDK5) on S245 (S273 in PPARγ2) is linked to obesity and promotes loss of insulin sensitivity, although the same authors a few years later identified other kinases phosphorylating this site, such as ERK.[13] They described several new compounds that block CDK5-mediated phosphorylation avoiding the typical side effects caused by PPARγ full activation. However, the exact structural mechanism through which CDK5, in complex with its

coactivator p25, is able to gain access to the PPARγ phosphorylation site, and what happens at structural level during PPARγ phosphorylation, has not yet been elucidated.

PPARγ is a "functionally pluripotent" protein because its activity is mediated by ligands that differentially affect the structural conformation and the dynamic properties of the protein. As a consequence, different biological pathways can be activated depending on the coactivator/corepressor recruited and the differential propensity for CDK5 to phosphorylate S245. Thus, to design novel potent antidiabetic agents, structural changes occurring during PPARγ phosphorylation need to be understood in detail. In this work we describe the mechanism underlying the CDK5/p25-mediated PPARγ phosphorylation providing a rationale for the inhibitory effect of certain ligands. In particular, we demonstrate that S245
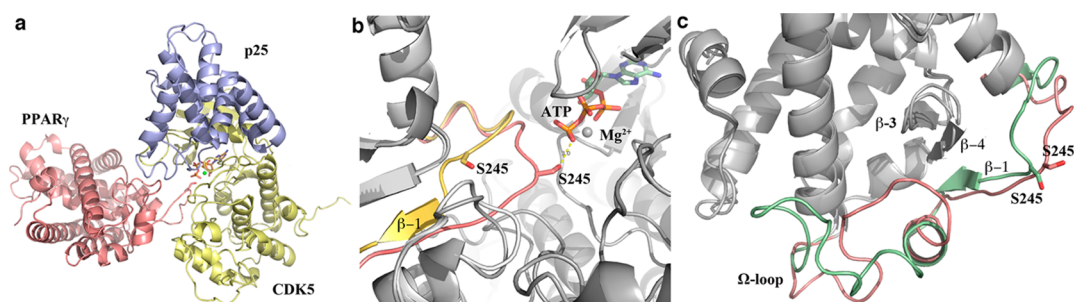
Figure 1. Docking study on the interaction between the CDK5/p25 complex and PPARγ: (a) model of the complex PPARγ/CDK5/p25/ATP/Mg^{2+} (CDK5/p25, PDB code 1H4L; PPARγ, PDB code 1PRG); (b) superposition of docked PPARγ (pink) and PPARγ (yellow) in its native state; (c) superposition of docked PPARγ (pink) to PPARγ (green) of the model 3 by M. Mottin (this model can be downloaded from the Supporting Information of ref 18).

within the putative PPARγ consensus motif SPFV (Supporting Information Figure S1) can only be accommodated in the active site of CDK5 through a transitory unfolding of the surface β-strand (β1), close to the consensus region. Moreover, we show an alternative, allosteric mechanism to block PPARγ phosphorylation via a hydrophobic cross-talk pathway in which the amino-terminal portion of H3 plays a pivotal role. Ligands bound in the hydrophobic region between H3 and the β-sheet, such as the *R* enantiomer of LT175[14] (named (*R*)-**1**), **7j**,[15] **3a**,[15] and MRL24,[12,17] block phosphorylation through a direct stabilization of the hydrophobic region between H3 and β1–β4. In contrast, ligands such as the *S* enantiomer of LT175,[14,16] which bind far from the consensus motif, between H11 and H3, are also able to inhibit S245 phosphorylation through a long distance allosteric mechanism that results in stabilization of the β-sheet.

■ RESULTS

To investigate the mechanism through which the CDK5/p25/ATP complex phosphorylates PPARγ, we employed a range of *in silico* and solution-based approaches suitable for studying such a transient, but critical, interaction.

Conformational Dynamics within PPARγ Are Essential to Enable Phosphorylation of S245 by CDK5/p25. In the past years, Mottin et al.,[18] by means of MD simulations, proposed four structural models of the complex between CDK5/p25 and PPARγ-LBD. According to these models, the authors identified two distal regions (PPARγ Ω-loop and β-sheet) in addition to the active site that may play an important role in the interaction of CDK5 with the nuclear receptor. Among these models, the authors chose the most stable (model 3) as the best candidate to represent PPARγ-CDK5/p25/ATP interaction, where the RMSF of the residues of the phosphorylation site is very low during the entire simulation.

Particularly, in the model proposed by Mottin et al., the external strand of the PPARγ β-sheet is quite distorted upon interaction with CDK5, with the disruption of one H-bond. Recently, Ribeiro Filho et al.[19] proposed a quite different model of the complex between CDK5/p25 and PPARγ-LBD. They found that PPARγ K261 occupies the P + 3 position of the consensus motif, forming a noncontiguous recognition site, as observed in other kinase substrates.[20] In this position, K261 forms a salt-bridge with E240 residue of p25 and might be responsible for the Cdk5 specifity. Moreover, they identify two other lysines, K263 and K265, located at the flexible H2′−H3 loop of PPARγ, pointing toward a region of Cdk5 that is rich in glutamic and aspartic residues (E/D rich region) and

interacting with it through salt-bridges. They validated the role of these lysines as crucial anchor residues in the PPARγ/Cdk5 interaction through single-point mutations (K261A, K263A, and K265A), phosphorylation test, and affinity studies. Finally, they identify by B-factor analysis a hydrophobic network of PPARγ residues (I341, M348, I249, and L255) which can be affected upon ligand binding, increasing the stability of H2′ and H2−H2′ loop and preventing a proper interaction with CDK5/p25. Particularly, they suggested a shift of the I341 side chain, induced by the ligand, toward M348 (β-sheet), I249 (H2−H2′ loop), and L255 (H2′) which could favor the stabilization of H2′ helix, as observed in their B-factor analysis.

We also investigated the structural interaction between the CDK5/p25 complex and PPARγ by means of *in silico* protein−protein docking. The known crystal structures of both the complex between CDK2 and cyclin-A, with bound ATP and a short peptide substrate[21] (PDB code 1QMZ), and the complex between CDK5 and p25 without the substrate[22] (PDB code 1H4L), were selected as templates for building a model of CDK5 in complex with ATP and p25 (CDK2/CDK5 sequence identity of 60%). Then, in order to model the interaction between CDK5/p25 and PPARγ, the phosphorylation motif of PPARγ was superposed to the corresponding consensus motif of the known CDK2 peptide substrate. This initial rough complex was subsequently optimized using the Rosetta version 3.4 protein docking protocol[23] (see methods section for details).

The obtained predicted complex (Figure 1a) indicated that the accommodation of PPARγ Ser-Pro motif into the active site of CDK5 is feasible only upon enlargement of the loop comprising the targeted residue for phosphorylation, i.e., S245, and H-bond engagement of S245 with K128 of CDK5 (corresponding to the homologous active site residue K129 of CDK2). This implies, in turn, that the neighboring strand of the β-sheet (β1) must undergo a transient unfolding in order to bring S245 close to the CDK5 active site (Figure 1b). In this hypothetical process, three H-bonds would be transiently lost (F247CO-F347N, I249N-F347CO, I249CO-T349N), with a loss of free energy that could be compensated by the H-bonds engaged between PPARγ and CDK5 and by phosphorylation of S245.

The model proposed here has some structural similarities to model 3 of Mottin (Figure 1c), with the exception of the Ω-loop conformation that is highly mobile. Particularly, model 3 of Mottin showed a partial unfolding of the surface β1 strand of PPARγ that is in agreement with the results of our docking

simulation, where this strand unfolds in a loop conformation. More interestingly, our model has striking similarities with that of Ribeiro Filho et al.,[19] in particular on the following points: (a) the position P + 3 of the PPARγ consensus motif is also occupied by K261 (and not by V248) which forms a noncontiguous recognition site (S245-P246-F247-K261); (b) K261, K263, and K265 are involved in electrostatic interactions with the Cdk5 E/D rich region by salt bridges; (c) the Ω-loop conformations of both models are very similar. Moreover, all three proposed models evidenced the crucial position of H2′ and H2−H2′ loop at the interface between PPARγ and CDK5/p25 (Supporting Information Figure S2).

Direct Link between Stabilization of the β-Sheet and S245 Phosphorylation. The double mutant F247C/G346C was expressed after a modeling study that confirmed the possibility of forming a stable disulfide bridge between the two cysteines belonging to the β-sheet (Supporting Information Figure S3). The disulfide bridge was meant to strongly stabilize the β-sheet, avoiding the transient unfolding of the β1 strand, with the aim to make S245 less available for the kinase. The mutant was equilibrated in the presence of a glutathione redox system (0.3 mM oxidized glutathione and 1.5 mM reduced glutathione) to help the formation of the disulfide bridge.[24] The predominance of the oxidized form of the mutant was checked and confirmed by the Ellman's test that quantifies the presence of free sulfhydryl groups in solution (Supporting Information Table 1). The comparison between the CD spectra of F247C/G346C and PPARγ WT showed that both proteins are correctly folded. In addition, the similarity of the CD spectra points to a very similar secondary structure content, with the preservation of the β-sheet (Supporting Information Figure S4 and Table 2). The further step was to perform the phosphorylation test checking the degree of phosphorylation of the double mutant. For detecting PPARγ phosphorylation rate the Pro-Q diamond phosphoprotein gel stain method has been used (see Experimental Section), avoiding in this way the use of specific antibodies. The results of the test (Figure 2) showed that the strong stabilization of the β-sheet prevents the phosphorylation of S245. This implies that different degrees of stabilization of the β-sheet by PPARγ ligands, full or partial agonists, may inhibit the S245 phosphorylation in a graded way. To check if the double mutation could affect the phosphorylation of S245, regardless of the formation of the disulfide bridge, the mutant was equilibrated in a buffer containing TCEP 1 mM in order to obtain a form of the protein with predominant free sulfhydryls. This form is also folded as the oxidized one (Supporting Information Figure S4 and Table 2). In Figure 2 it is shown that the predominant reduced form of the mutant (after equilibration with TCEP 1 mM) is able, unlike the oxidized form, to phosphorylate S245 as the WT, although to a lesser degree.

LT175 Is an Allosteric Inhibitor of PPARγ Phosphorylation. The following step was to test the capability of inhibiting the S245 phosphorylation of some PPARγ ligands (7j, 3a, MRL24, LT175, and rosiglitazone) whose different binding mode to the PPARγ LBD is known.

Starting from the observation that 7j and 3a have a very similar structure and bind similarly to PPARγ, unless their terminal aliphatic chain that in 7j faces the β-sheet whereas in 3a it occupies a different region of the LBD (Supporting Information Figure S5), we tested their potency as inhibitors of PPARγ phosphorylation with the aim to observe if the different stabilization of the β-sheet could affect the phosphorylation
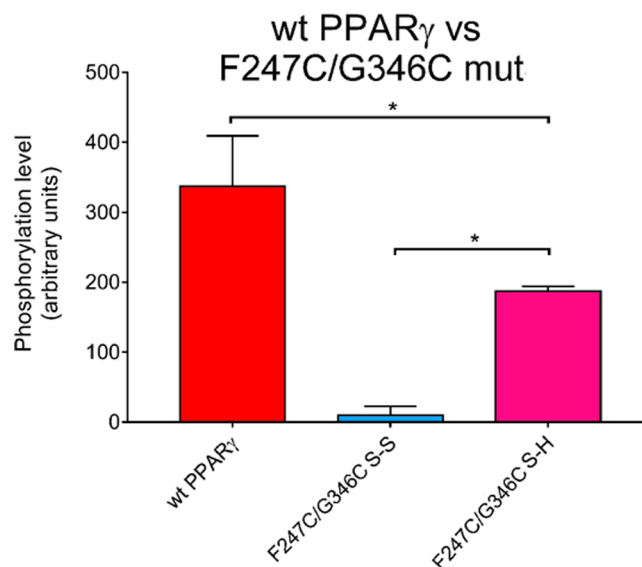
**Figure 2.** Phosphorylation level of double mutant F247C/G346C PPARγ. Comparison between S245 phosphorylation of WT PPARγ, F247C/G346C (S−S) PPARγ, and F247C/G346C (SH) PPARγ. Phosphorylation level was evaluated by using the phospho gel stain method. For each condition tested the intensity of the protein incubated in the absence of kinase was subtracted from that obtained in the presence of kinase and values obtained were normalized to the amount of protein loaded. Data represent the mean of at least three measurements, and error bars indicate SD. Ligand concentrations were 10 μM. All data were analyzed by one-way ANOVA with multiple comparisons followed by Dunnet test. In all cases, $P < 0.05$ was considered statistically significant ($* = P \leq 0.05$, $*** = P \leq 0.01$).

degree. The results showed that 7j, able to better stabilize the β-sheet with both disordered conformations of its aliphatic chain, inhibits the phosphorylation to a greater extent than 3a (phosphorylation level of 14% vs 36%) (Figure 4 upper panel).

MRL24, which also occupies the same region of the 7j aliphatic chain (Figure 3a) between H3 and the β-sheet, strongly inhibits the phosphorylation (32%). Surprisingly, LT175, which binds PPARγ LBD in the region between H11 and H3, far from the phosphorylation site (Figure 3b), also inhibits the phosphorylation and better than the reference molecule rosiglitazone[25] (phosphorylation level of 47% vs 65%). These results were also confirmed by an ELISA protocol (enzyme-linked immunosorbent assay) where the inhibition by LT175 was comparable to that by its enantiomer (R)-1, bound to the LBD similarly to MRL24 (Supporting Information Figure S6). The results of these experiments let us hypothesize a long-distance inhibition mechanism of PPARγ phosphorylation induced by LT175.

The Supporting Information Figure S7 shows the phosphorylation of histone H1, with or without LT175, and demonstrates that the ligand does not inhibit Cdk5 through a direct interaction.

Structural Mapping of the Allosteric Inhibition Mechanism of PPARγ Phosphorylation by CDK5. We carried out a 2D ^{1}H−^{15}N HSQC NMR experiment to map the effect of the ligand binding event on the PPARγ backbone chemical shifts and compared the spectra with that of apo-PPARγ. For this aim we analyzed several compounds with different potency and bound to different regions of the PPARγ LBD (LT175, GW1929,[26] rosiglitazone) (Figure 5a).
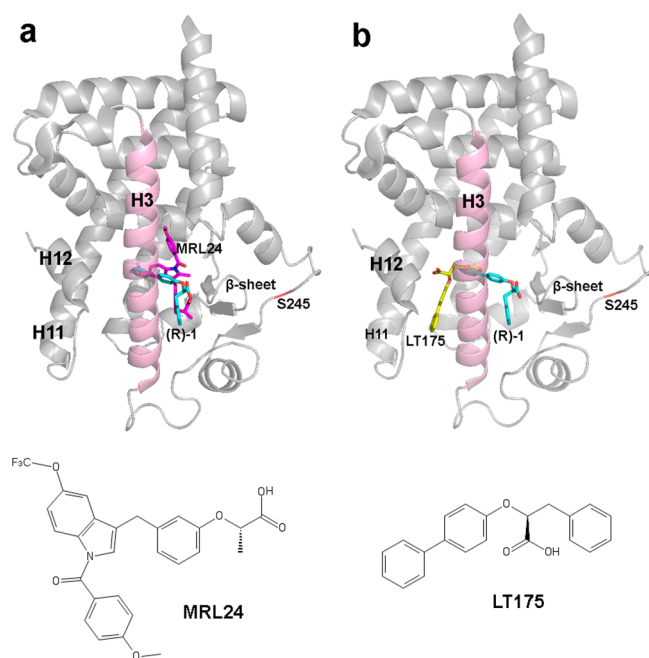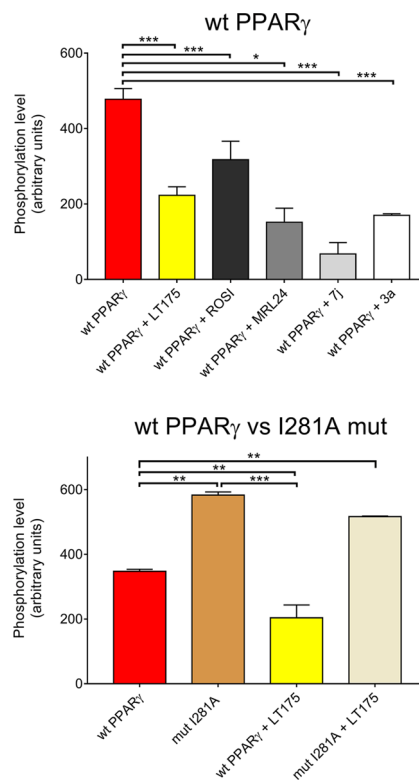
Figure 3. Comparison between different ligand binding modes in the PPARγ-LBD: (a) superposition of (R)-**1** (cyan) and MRL24 (purple); (b) superposition of LT175 (yellow) and (R)-**1**. The phosphorylation target, S245, is shown in red, helix3 in pink, and the β-sheet in light blue. PDB codes of LT175, (R)-**1**, and MRL24 structures are 3B3K, 3D6D, and 2Q5P, respectively.

Figure 4. Phosphorylation level of PPARγ and I281A mutant in the presence of different ligands. Upper panel shows inhibition of the phosphorylation on WT PPARγ LBD by LT175 and other ligands. Lower panel shows inhibition of the phosphorylation on the mutant I281A LBD by LT175. The phosphorylation degree of I281A was ∼60% higher than the WT, confirming that the mutation does not prevent the phosphorylation. Phosphorylation level was evaluated by using the phospho gel stain method. For each condition tested the intensity of the protein incubated in the absence of kinase was subtracted from that obtained in the presence of kinase and values obtained were normalized to the amount of protein loaded. Data represent the mean of at least three measurements, and error bars indicate SD. Ligand concentrations were 10 μM. All data were analyzed by one-way ANOVA with multiple comparisons followed by Dunnet test. In all cases, $P < 0.05$ was considered statistically significant ($* = P \leq 0.05$, $*** = P \leq 0.01$).

We focused our attention on the cross-peak related to M348, a residue located on the β4 strand, directly linked to helix 3 through vdW interactions (about 4 Å from I281). The M348 cross-peak, which could be easily assigned in the spectrum, was slightly shifted in the presence of rosiglitazone, as already observed by T. S. Hughes and co-workers,[27] and of GW1929 (Figure 5b). This is in accordance with the observation that both ligands have an aromatic ring close to the M348 side chain. In the presence of LT175, bound very far from the M348 side chain and the phosphorylatable S245 (about 20 Å), we observed a marked change of M348 chemical shift (Figure 5b). To go more in depth, we performed titration experiments with LT175 ranging from 0.1 to 1 mol equiv and we observed the M348 peak getting gradually weaker in intensity until it disappeared at 1 mol equiv and the concomitant appearance of a new M348 peak in the spectrum (Supporting Information Figure S8). This suggested that M348, despite the long distance from the ligand, is strongly affected by LT175 binding through a hydrophobic cross-talk pathway running from the ligand up to the β-sheet, via I281 on H3.

The central position of I281 in this pathway led us to hypothesize a crucial role of this residue in the molecular cross-talk and that its mutation to I281A might interrupt the hypothesized signaling mechanism. We then mutated I281 to Ala and compared the NMR spectrum of apo-I281A to that of apo-WT, observing only a negligible change in the chemical shift of M348 and the close Y222 (Figure 5c).

When comparing the spectrum of I281A PPARγ apo to that of its complex with LT175, we observed that the M348 cross-peak did not shift (Figure 5d). This confirms that the residue I281 could be crucial for the signaling pathway. We performed SPR experiments to confirm that LT175 also binds to the I281A mutant with similar affinity to that of WT. The SPR results

(Supporting Information Figure S9) show that LT175 binds I281A and WT with a similar affinity (K_a of 3.7×10^5 versus 5.5×10^5 M^{-1}). The kinetic data (Figure S9 of Supporting Information) indicate a greater flexibility of the mutant as LT175 associates and dissociates faster with the mutant than with WT (3 and 4 times, respectively).

To investigate the stability of the holo mutant, circular dichroism (CD) experiments were then performed. CD shows that the mutant is as stable as the WT, but in the presence of the ligand it is stabilized much weaker than WT, which, on the contrary, results in being strongly stabilized (Figure 6a,b). Also these data reflect an allosteric structural coupling via I281 between the ligand binding region, delimited by H3 and H11, and the β-sheet.

On the basis of the so far acquired experimental and computational data, a cross-talk mechanism has been hypothesized as shown in Figure 7. As already known, upon binding of LT175, the side chain of F282 is considerably shifted from its original position (Supporting Information Figure S10) as observed in the apo-form, allowing a vdW interaction with
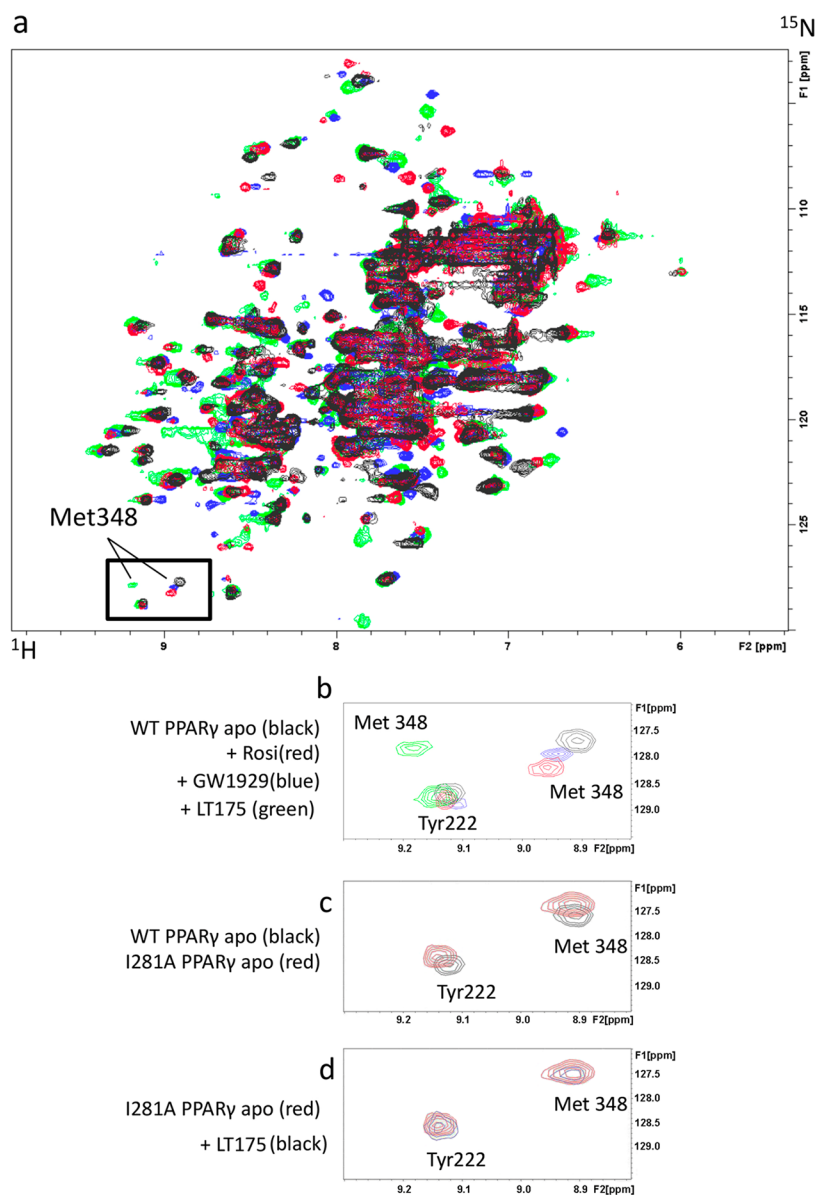
Figure 5. (a) $^{1}H-^{15}N$ HSQC NMR spectra: black, blue, red, and green peaks show apo PPARγ-LBD, PPARγ + GW1929, PPARγ + rosiglitazone, and PPARγ + LT175, respectively; (b) superimposed $^{1}H-^{15}N$ HSQC spectra of WT PPARγ apo (black), PPARγ + rosiglitazone (red), PPARγ + GW1929 (blue), and PPARγ + LT175 (green); (c) superimposed $^{1}H-^{15}N$ HSQC spectra of WT PPARγ apo (black) and I281A mutant apo (red); (d) superimposed $^{1}H-^{15}N$ HSQC spectra of I281A mutant apo (red) and in the presence of LT175 (black). The concentration of the ligands was 1 mol equiv.

the L356 side chain.[14] This would trigger the signal, via L356, L353, and I281, up to M348 on the strand β4, I249 on β1, and L255 on H2′ (Figure 7).

I281 Has a Pivotal Role in Allosteric Blocking of PPARγ Phosphorylation. In order to confirm the proposed pathway from F282 to S245, we repeated the phosphorylation assay on the mutant I281A.

Our attempts to mutate other residues involved in the cross-talk pathway were fruitless because the mutants were unstable or difficult to express. Conversely, the I281A mutant has the same stability as wild-type PPARγ, as shown by CD results (Figure 6).

Consistent with our hypothesis, we observed in the mutated protein a significant decreasing of the phosphorylation inhibition upon ligand binding (Figure 4 lower panel and Supporting Information Figure S11), demonstrating that a

break in the molecular cross-talk pathway disfavors the stabilization of the β-sheet and lowers the inhibitory potency of LT175. It is important to observe that I281A mantains the ability to phosphorylate S245, even to a greater extent than the WT as shown in the Figure 4 lower panel.

LT175 Stabilizes H3. Molecular dynamics simulations of the wild-type PPARγ in its apo and holo forms with LT175 were carried out to study conformational dynamics of the PPARγ structure with and without ligand. To this end, a 200 ns simulation, typically, of both the apo and holo PPARγ was performed to investigate the role played by the key residues Phe-282 and Ile-281, belonging to H3, in PPARγ stability and to confirm the hypothesized hydrophobic pathway from the ligand to the β-sheet and S245, via H3. Analysis of the equilibrated part of the simulations (see methods section) showed that global flexibility (RMSF) of wild type PPARγ in
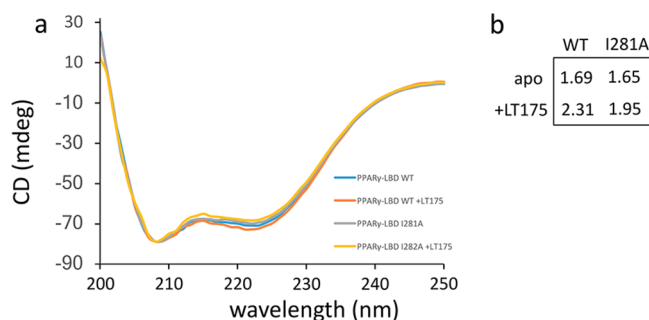
Figure 6. Biophysical characterization and evaluation of PPARγ WT and I281A with or without LT175: (a) PPARγ (20 μM) spectra of circular dichroism (CD) from 200 to 250 nm; (b) results of denaturation experiment using GdmCl (0, 0.5, 1.0, 2.0, 3.0, 6.0 M). Each value indicates guanidine concentration to achieve 50% of folded protein, calculated by Boltzmann function in the software Prism.
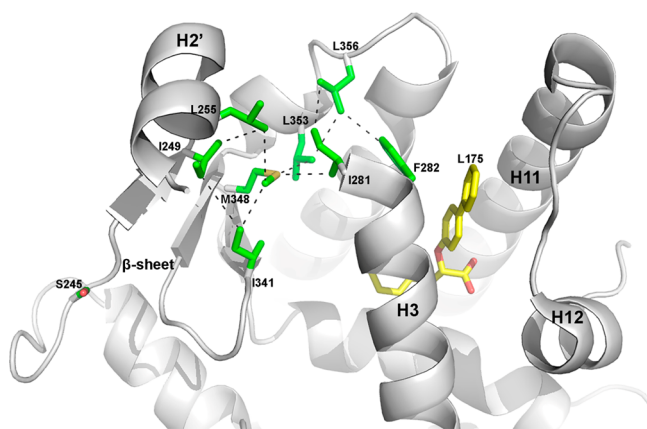
Figure 7. Hypothesis of allosteric inhibition by LT175, showing hydrophobic signaling pathway from the ligand to S245.

the presence of ligand was reduced with respect to the apo counterpart. As shown in Figure 8a, a general decrease of the RMSF values was observed upon ligand binding for the wild-type PPARγ throughout its structure, the only exception being a short loop encompassing residues 269–274 (ω-loop), thus suggesting that the reduced accessibility of the phosphorylated Ser-245 to the bulk solvent could be ascribed to the increased compactness of the protein structure.

To get a deeper insight into the molecular mechanism of protein stabilization upon ligand binding, the role played by specific residues connecting the ligand binding pocket to the phosphorylated loop hosting Ser-245 was investigated by dihedral angles analysis throughout the simulations. The results are shown in Figure 8b,c.

The figure reports the population distribution of the χ_1 dihedral angles in the equilibrated portions of the trajectories for Phe-282 and Ile-281. As shown, Phe-282 adopts two distinct χ_1 population distributions with and without ligand. This suggests that in apo-PPARγ the Phe-282 side chain is located in correspondence of the phenyl moiety of LT175, while binding of LT175 forces Phe-282 side chain to adopt a different conformation, where the phenyl ring makes strong hydrophobic contacts with Ile-281.

In turn, the distribution of χ_1 populations of Ile-281 revealed a more complex behavior: in apo-PPARγ Ile-281 χ_1 adopts three different modal values (i.e., −60, 60, and 180); upon ligand binding and engaging hydrophobic interactions with Phe-282, the distribution of the Ile-281 χ_1 angles is restrained to a bimodal value, being the population centered at −60° almost canceled out. This suggests that LT175 binding to PPARγ causes a rearrangement of the PPARγ hydrophobic interactions at the Ile-281/Phe-282 site, resulting in a reduction of the conformational freedom of Ile-281. The latter is indeed at contact distance with Met-348, which belongs to a cluster of hydrophobic residues (including M348, I341, and I249) connecting the β-sheet to the loop hosting Ser-245. The change in conformational dynamics of PPARγ upon LT175 binding was detected by analyzing the cross-correlations and concerted motions calculated using essential dynamics (ED) that provides principal directions of fluctuations where protein motion is likely to occur. ED analysis showed that the reduction in protein conformational flexibility by ligand binding was not only a global effect on PPARγ (Supporting Information Movies 1 and 2) but it affects specifically the structural integrity of the strand β1, close to Ser-245, thus affecting its phosphorylation rate as well. Therefore, the MD results seem to confirm our hypothesis of the hydrophobic cross-talk pathway running from the ligand LT175 up to the S245, via I281 on H3 and M348 on β4.

HDX-MS. Hydrogen/deuterium exchange/mass spectrometry[28] (HDX-MS) was used to also probe the conformational changes remote from the ligand binding site with the aim to confirm the allosteric mechanism of inhibition of CDK5-mediated PPARγ phosphorylation by LT175. We ran the experiment on both WT PPARγ and I281A PPARγ in order to probe the pivotal role of this residue in the hydrophobic signaling pathway.
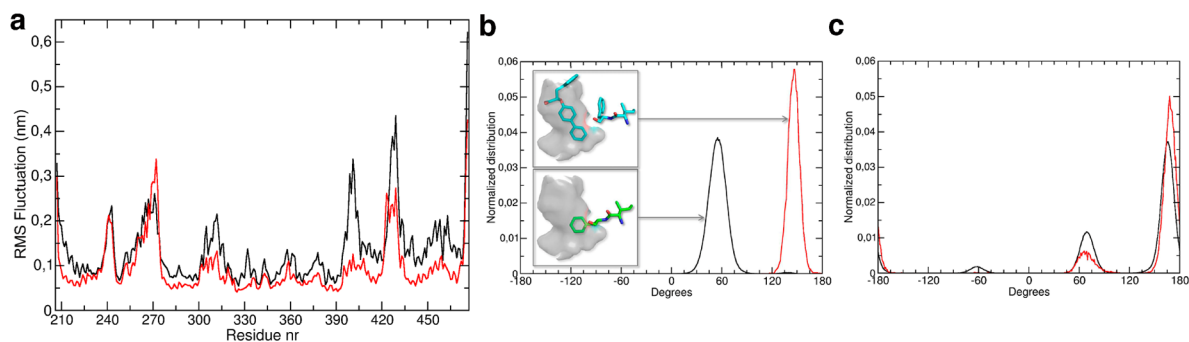
Figure 8. Molecular dynamics simulation: (a) RMSF (nm) of α carbon atoms as a function of residue number; (b) Phe282 χ_1 dihedral angles distribution, as calculated on the equilibrated part of all simulations; (c) I281 χ_1 dihedral angles distribution. A schematic representation of Phe-282 average position for the two distribution is also shown in the insets. Black: apo PPARγ. Red: holo PPARγ with LT175.
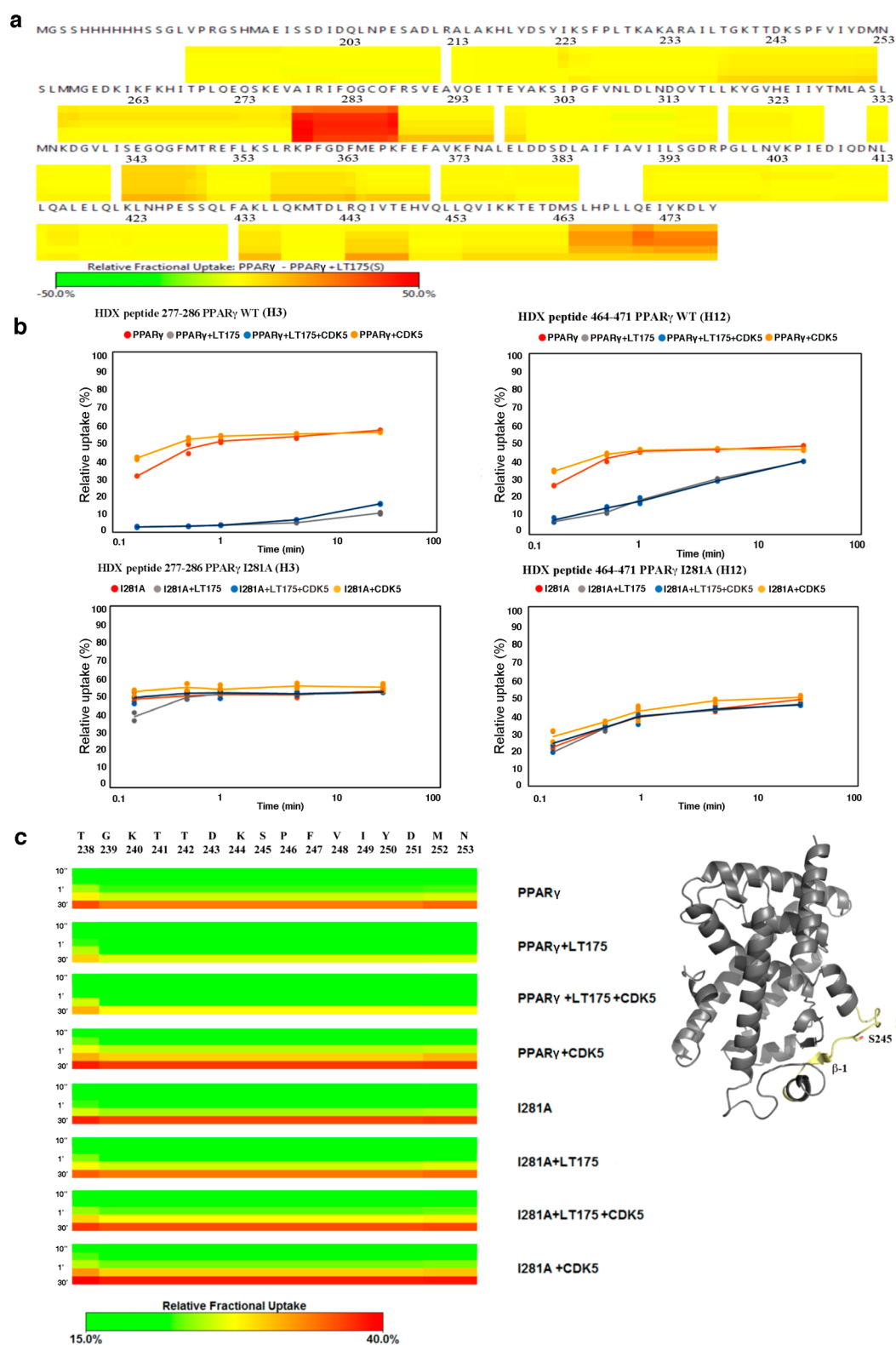
Figure 9. HDX-MS analysis. (a) Heat map showing a comparison between PPARγ in the presence or absence of LT175 where the relative uptake of PPARγ + LT175 is subtracted from PPARγ. The red areas represent an increased uptake, the green areas a decreased uptake, the yellow areas an unaffected uptake by the addition of LT175. Every bar is composed of five lines representing from top to bottom the time points 10 s, 30 s, 1 min, 5 min, and 30 min. (b) Deuterium relative uptake of peptides VAIRIFQGCQ (277−286) in PPARγ and VAIRAFQGCQ (277−286) in mutated PPARγ I281A and SLHPLLQE (464−471). (c) Highlight of the segment containing S245 in all the tested conditions.

Exchange dynamics of various segments was monitored by measuring the deuterium content of the corresponding pepsin induced peptide fragments. A sequence coverage of 92.4% was achieved (Supporting Information Figure S12). Comparative H/D exchange heat maps of WT PPARγ in the presence or

absence of LT175 overall did not reveal any significant changes, with the exception of two specific regions (Figure 9a).

In the region 277−286, corresponding to the amino-terminal portion of H3 and containing the residue I281, the deuterium uptake decreases considerably in the presence of LT175, whereas these effects are not observed in mutated PPARγ I281A (Figure 9b). This observation confirms the key role of both the initial part of H3 and the residue I281 in the molecular cross-talk pathway. As known, the binding of LT175 in the "diphenyl pocket" provokes the conformational switch of F282 side chain from *trans* to *gauche** conformation (Supporting Information Figure S10) and in turn a vdW interaction of this residue with the L356 side chain (Figure 7). The mutation I281A breaks this interaction, making this region less stable, as confirmed by our HDX. The other change in deuterium uptake concerns H12, which, as expected, is better stabilized by LT175 through H-bonds with Y473 (Figure 9a,b and Supporting Information Figure S13). Interestingly, LT175 is not able to stabilize H12 in the mutant I281A (Figure 9b and Supporting Information Figure S13), demonstrating once more the importance of the initial part of H3 (I281 and F282) as a fundamental pivot in the communication among distant regions of the LBD.

A minor but significant change in the deuterium uptake was observed in the region of the external (β1) strand of the β-sheet. Considering the relative fractional uptake of PPARγ and PPARγ + CDK5 in the range +15.0% to +40.0%, it is evident that LT175 stabilizes this region in PPARγ WT but not in the mutant (Figure 9c). This confirms that the mutation I281A breaks the molecular cross-talk pathway (Figure 7).

LT175 Does Not Bind the Alternative Site of PPARγ. As known, some PPARγ ligands are able to bind an alternative low-affinity site, especially at high concentrations.[29−33] To exclude that the inhibition of phosphorylation by LT175 was caused by the binding of the ligand to the alternative site, close to the β-sheet, and not by the described allosteric mechanism, we set up the following experiment. The small ligand GW9662,[30] known to covalently bind PPARγ to C285 preventing in this way the canonical binding of LT175 (Supporting Information Figure S14), was preventively equilibrated with PPARγ. An SPR experiment was then performed after immobilizing PPARγ/GW9662 on the chip, allowing LT175 to flow into the cell at the concentrations of 0.1, 1, 10, and 100 μM. The sensograms showed that at the concentrations used in the phosphorylation experiments (0.1, 1, and 10 μM) LT175 does not bind PPARγ and only at the high concentration of 100 μM is able to bind the low affinity alternative site (Supporting Information Figure S15).

■ DISCUSSION

This work extends several of our previous studies where we evidenced new structural features of PPARγ in the crystal complex with a new series of ligands that, interacting with different regions of the LBD, confer a differentiated biological response in cell and animal models.[34−39]

In particular, we provided a rational explanation of how some PPARγ ligands affect the CDK5-induced phosphorylation rate by increasing the stability of the β-sheet and decreasing the dynamic nature of the nuclear receptor depending on their binding mode.

To elucidate this mechanism, we explored in depth the dynamics of the CDK5 approach to PPARγ consensus region through the integration of a number of biophysical techniques including NMR and hydrogen/deuterium exchange/mass spectrometry (HDX-MS) and observed how the ligand binding affects the inhibition rate of CDK5-mediated PPARγ phosphorylation.

In particular, we started from the hypothesis, suggested by the docking simulation, that the accommodation of PPARγ consensus region in the active site of CDK5 is possible only if a transitory unfolding of the PPARγ-LBD β1 strand occurs. The partial unfolding of β1 is further supported by the observation that in the PPARγ-homologous nuclear receptor RAR[40] and in almost all nuclear receptors the corresponding β-strand is replaced by a loop (17 residues in the case of RAR), thus suggesting that this region is not essential for the global stability of the LBD.

As a consequence of this premise, the increase in the stability of the β-sheet should correspond to a decrease in S245 phosphorylation.

A double mutant, designed to have a disulfide bridge that strongly stabilizes the β-sheet, confirmed that the phosphorylation of S245 is completely inhibited if the transient unfolding of β1 strand by Cdk5 is prevented. As shown by Ribeiro Filho et al.,[19] the stabilization of the helix H2′ and the loop H2−H2′ at the interface between PPARγ and Cdk5/p25 can also affect the phosphorylation rate.

This is in accordance with the observation that ligands bound at the hydrophobic region between H3 and β1−β4 of PPARγ, such as 7j, the partial agonists (R)-1,[14] MRL24,[12,17] and nTZDpa,[41] are able to reduce the mobility of this region through vdW interactions (Supporting Information Figure S16) or H-bonds with the β3−β4 strand (S342), inhibiting the phosphorylation of S245 by CDK5.

Then, the direct stabilization of the β-sheet by interactions with residues of the internal strands of the β-sheet (β3−β4), the helix H2′, and the loop H2−H2′ makes S245 less available for the kinase and represents the main strategy to block PPARγ phosphorylation. Also full agonists, such as rosiglitazone that possesses a terminal tail in front of β4, are able to stabilize the β-sheet through vdW interactions (Supporting Information Figure S17) inhibiting the phosphorylation, although to a lesser extent. In this regard, it is interesting to note that the small-size antagonist of PPARγ, SB1404[29] (PDB code 5DV6), covalently bound to C285 in the canonical binding pocket, is not long enough as rosiglitazone to reach β4 and does not inhibit the phosphorylation of S245. Similarly, 3a, whose long aliphatic chain, unlike 7j, does not face the β-sheet, inhibits the phosphorylation to a lesser extent than 7j (Figure 4, upper level). In the same way between the two enantiomers SB1494 and SB1495[42] (PDB codes 6IJS and 6IJR, respectively), the first bound in the region between H3, H2′, the β-sheet, and the ω-loop, the second in a different region far from the β-sheet, only the first is able to inhibit the phosphorylation of S245 (Supporting Information Figure S18). On the contrary, less clear was the case of LT175[14] that, although occupying a region far from the consensus motif, also decreases the phosphorylation rate.

Specifically, here we demonstrate that a long distance allosteric mechanism to block PPARγ phosphorylation is possible. Indeed, LT175 by occupying a new branch of the LBD, named "diphenyl pocket", displaces the side chain of F282 that, by switching from *trans* to *gauche** upon ligand binding, triggers a hydrophobic cross-talk (Figure 7). This pathway passes through several hydrophobic residues belonging to H3, H6, and the β-sheet and arrives up to S245, making it

less available to phosphorylation by CDK5. This hydrophobic cross-talk can also extend up to H2′ and H2−H2′ loop, via residues I341 and M348, altering their stability and preventing a proper interaction with Cdk5/p25, with a consequent decreased phosphorylation[19] (Figure 7 and Supporting Information Figure S2). The crucial role of M348 for the stabilization of the β-sheet, the H2−H2′ loop, and H2′ helix was also confirmed by the marked change of its chemical shift, upon ligand binding, observed in the previously described NMR experiment.

It is interesting to note that in this allosteric mechanism a central role is played by H3 that allows distant regions to communicate with each other, as shown by both site-specific mutagenesis and HDX experiments.

Although blocking of phosphorylation can be mediated by ligand allostery directly from ligand to the kinase binding surface of PPAR, there are also other inhibition mechanisms such as the one proposed by Li et al.,[43] where NCoR tethers the kinase into the transcriptional complex.

CONCLUSIONS

In this work two different ways to alter the dynamics of the β-sheet affecting S245 phosphorylation have been shown:

(i) a mechanism of more direct stabilization of the β-sheet, H2′ and H2−H2′ loop, as realized by most ligands with reduced agonist activity, such as MRL24, but also by full agonists, such as rosigitazone, long enough to interact with the β4 strand;

(ii) a long distance allosteric mechanism, as in the case of the partial agonist LT175, by which a similar stabilization of the β-sheet can be obtained, leading to an equally effective inhibition of Ser-245 phosphorylation. It is evident that in both cases the rate of inhibition is not correlated to the degree of ligand agonism but rather to its ability to stabilize the β-sheet through H-bonds or vdW interactions. As shown by Choi et al.,[11] this inhibition leads to the recruitment of a different set of coactivators that provoke an increase of the expression of insulin sensitizing genes, such as adiponectin. This may explain why PPARγ partial agonists, such as MRL24, or nonagonists can exhibit similar or higher antidiabetic effects than those of full agonists, whereas the classical agonism is not required for strong antidiabetic action but is rather associated with the occurrence of undesired side effects. These general considerations may provide a new structural strategy for designing of antidiabetic drugs acting on PPARγ.

EXPERIMENTAL SECTION

General Information. The compounds used in this work have a purity of ≥95% (Table 3 of Supporting Information).

Site-Directed Mutagenesis. The PPARγI281A mutant was cloned in pET-28 plasmid for *Escherichia coli* expression. The QuickChange site-directed mutagenesis kit (Stratagene) was used to introduce the point mutation into the bacterial expression vector. The forward primer for the mutation I281A was 5′-gtggccatccgcgcctttc-agggctgc-3′, and the reverse primer is the exact complement of the forward primer. The PPARγ double mutant F247C/G346C was generated by two successive QuickChange site-directed mutagenesis events to introduce the mutations. Sequences of the forward primers, with the altered residue underlined, were as follows: F247C 5′-ggaaagacaacagacaaatcaccat*gc*gttatctatgacatgaatt-3′; G346C 5′-ctcatatccgagggccaat*gc*ttcatgacaaggg-3′; the reverse primers used are the exact complements of the forward primers. DNA sequencing was performed to confirm the presence of the desired mutations.

Protein Expression and Purification. The ligand-binding domain of human PPARγ (NP_001120802; aa 207−474), I281A, and the double mutant F247C/G346C were expressed as N-terminally His-tagged proteins using pET-28 vector and were purified as previously described.[35] For NMR experiments, the expression plasmid was transformed into *E. coli* Rosetta (DE3) pLysS cells (Invitrogen) and grown at 37 °C in a M9-based medium containing 34 μg/mL kanamycin supplemented with ^{15}NH$_4$Cl (Cambridge Isotopes). When the cell density reached OD$_{600nm}$ of ∼0.6, protein expression was induced with 0.5 mM isopropyl β-D-thiogalactoside (IPTG) and cells were grown for 18 h at 20 °C, harvested by centrifugation. Cells were lysed by sonication in buffer A containing 20 mM Tris-Cl, pH 8.0, 100 mM NaCl, 2 mM TCEP, 1 mM 4-(2-aminoethyl)benzenesulfonyl fluoride hydrochloride (AEBSF), and protease inhibitor cocktail (Nacalai Tesque). After centrifugation the supernatant was applied to a Ni-NTA agarose column (QIAGEN), and the His-tagged protein was eluted with buffer A containing 250 mM imidazole. The His-tag was removed by overnight digestion with TEV protease (Nacalai Tesque) at 25 °C. The PPARγ LBD was further purified on a Resource Q column (GE Healthcare) using a 0−1.0 M NaCl gradient in buffer A followed by gel filtration on a Superdex S75 in 20 mM Tris-Cl, pH 8.0.

NMR. ^{1}H−^{15}N heteronuclear single quantum correlation (HSQC) spectra were collected at 25 °C on Bruker AV600 spectrometer equipped with a cryoprobe accessory. A NMR sample containing 0.3 mM ^{15}N labeled PPARγ LBD, 0.03−0.3 mM ligand-bound, labeled PPARγ LBD in a NMR buffer (5% D$_2$O, 0.05% sodium azide, 20 mM potassium phosphate, pH 7.4, 50 mM KCl, 8 mM β-mercaptoethanol-d_6, and 0.5 mM EDTA-d_{16}) was prepared as described.[44]

The chemical shift for Met348 was assigned using BMRB entries 15518[44] and 17975.[28]

***In Vitro* Kinase Assay.** The assay was performed on the double mutant F247C/G346C, and both the WT-PPARγ and I281A-PPARγ LBDs, in the apo-form and in the complex with LT175 and other ligands (rosiglitazone, **7j**, **3a**, MRL24, and (*R*)-**1**). For the kinase assay, stock solutions of ligands were prepared by diluting with 100% DMSO to a concentration of 500 μM. The stock solutions were further diluted with 50 mM Tris-HCl, pH 7.5, up to the final concentration of 10 μM and pre-equilibrated overnight at 4 °C with the protein.

Kinase assay was carried out at 30 °C for 2 h in 50 μL volume buffer containing 50 mM Tris-HCl, pH 7.5, 1.2 μg of PPARγ, 10 μM ligand, 2.5 mM MgCl$_2$, 50 μM DTT, 500 μM ATP, 60 ng of CDK5/p35 (Sigma-Aldrich code no. SRP5011).

Pro-Q Diamond Phosphoprotein Gel Stain. Pro-Q diamond phosphoprotein gel stain provides a convenient method for selectively staining phosphoproteins in acrylamide gels, without the need for blotting or use of phosphoprotein specific antibodies. After performing electrophoresis and reading results with Pro-Q diamond phosphoprotein gel stain (ChemiDoc), a further step of gel staining with SYPRO Ruby protein gel stain was performed in order to ascertain the relative phosphorylation state of proteins for normalization. More detailed information on the protocol used in this experiment can be obtained at the Thermofisher site.

ELISA of PPARγ Phosphorylation. Polystyrene microwell plates (Nunc immuno-plate Maxisorp 96-well, Sigma code M9410) were coated with the reaction mixture. After overnight incubation at 4 °C, the coated wells were washed three times with WB (PBS + Tween 0.005%) and left to block in PBS containing 1% bovine serum for 90 min at 37 °C. The wells were then washed three times with WB, and 100 μL of anti-phospho-Ser/Thr-Pro antibody (Sigma-Aldrich code no. A05368) diluted 1:500 in PBS was added to the wells and incubated for 60 min at 37 °C.

The wells were washed three times with WB, and 100 μL of anti-mouse IgG (whole molecule)-peroxidase antibody produced in goat (Sigma-Aldrich code no. A4416) diluted 1:1000 was added to the wells. After 60 min of incubation at 37 °C, the wells were washed three times with WB, and 200 μL of o-phenylenediamine dihydrochloride (Sigmafast OPD code no. P9187) dissolved in water was added to the wells. Optical density (OD) was measured at 450 nm using Apply Scan Thermofisher Reader, and the data were processed using Excel.

Ellman's Assay. The Ellman's assay kit measures sulfhydryl groups with the thiol reagent 5-5dithiobis[2-nitrobenzoic acid] (DTNB), which forms the 5-thionitrobenzoic acid and a mixed disulfide. Under conditions of oxidative stress, free sulfhydryls decrease and disulfides increase. Further information on the protocol used in the experiment can be obtained by consulting the Thermo Scientific site.

CD Analyses. The CD spectra of PPARγ wild type and the double mutant F247C/G346C, both in the reduced (+TCEP) and oxidized form, were recorded at 20 °C using a Jasco J-810 spectropolarimeter equipped with a Peltier thermostatic cell holder. Far-UV measurements (190−260 nm) were carried out using a 0.1 cm path length cell in 20 mM Tris-HCl, 0.5 mM EDTA, pH 7.5, at a protein concentration of 10 μM.

GuHCl Denaturation Experiment. GuHCl (≥99%) was purchased from Nacalai Tesque (Kyoto Japan). In each GuHCl denaturation experiment, samples of PPARγ were titrated with GuHCl from 0 to 6.0 M at a protein concentration of 20 μM. Unfolding was initiated by dilution of a concentrated protein stock into the appropriate GuHCl buffer. All samples were incubated at 20 °C for 2 h before measurement using a JASCO J-1500 CD spectrometer.

Model of the Complex CDK5/p25/ATP/Substrate and Protein−Protein Docking. To generate a model for the complex CDK5/p25/ATP, the homologous protein CDK2 (PDB code 1QMZ) was chosen as template for comparative modeling[45] of the target protein CDK5 because it is the only known crystallographic structure of CDKs family available in the PDB in the complex with a substrate. Moreover, CDK2 and CDK5 share almost 60% of sequence identity in different species.[22] After cleaning the PDB files, the sequence of the target protein was threaded onto the three-dimensional backbone of the template structure according to the sequence alignment of the two proteins. Areas in which the template and the target sequence diverged substantially were remodeled and refined by using the Rosetta loop-building CCD algorithm. Loop coordinates for missing density in the threaded model were generated from fragment libraries obtained from both Robetta (http://robetta.bakerlab.org/fragmentsubmit.jsp) and Fragment Picker applications. To energetically minimize the Rosetta model, the Rosetta relax protocol was followed. Once the model of the target protein CDK5 was built, to generate the model of CDK5/p25/ATP/substrate, the peptide described by Brown et al.[21] was used as template for the substrate and the file saved as PDB. The superposition was performed by PyMol[46] and the energy minimization by MOE software.[47]

Once a putative model for the complex CDK5/p25/ATP/substrate was created, it was manually superposed by PyMol to its docking partner PPARγ so that the segment containing the residues S245 and P246 was exactly superimposed to the consensus peptide ASP described by Brown et al.[21] A new file containing both the complex between CDK5/p25/ATP and its docking partner PPARγ was thus created, and Rosetta version 3.4 software was used to predict the bound structure of PPARγ/CDK5/p25/ATP complex starting from the model. To run the Rosetta protocol for protein−protein docking, a distance constraint file between PPARγ-S245 and CDK5-K128 needed to be created. The position found in the low-resolution search was optimized by rigid body Monte Carlo minimization before running the high-resolution docking.

Molecular Dynamics. All simulations have been performed using Gromacs 2016.1. The structures were centered in cubic boxes with minimum distance of 1.5 nm between each atom of the protein and the box. The SPC water model was used to solvate the systems. Ionic strength was adjusted to make sure all simulation were electrically neutral. MD simulations were performed with periodic boundary conditions in the isothermal−isochoric ensemble (*NVT*), using an integration step of 2 fs and keeping the temperature constant at 300 K by using the velocity rescaling algorithm.[48] Electrostatic interactions were treated using the particle mesh Ewald method[49] for the long-range contribution (reciprocal space) and with a cutoff radius of 1.0 nm. The Amber99b force field[50] was used. Before production runs, all systems were subject to a minimization cycle and thermalization procedure to bring gradually the temperature to 300 K. All runs consisted of at least 190 ns MD simulations in a *NVT* ensemble.

Essential Dynamics analysis was performed according to Amadei et al.[51] Basically, atomic positional fluctuations covariance matrix was built on the equilibrated portion of all trajectories and diagonalized to get principal components representing large amplitude motions sampled during simulation time. Trajectories were projected onto selected eigenvectors to show main dominant protein motions. Figures were generated using the Visual Molecular Dynamics software (http://www.ks.uiuc.edu/Research/vmd/).

Hydrogen/Deuterium Exchange Coupled with Mass Spectrometry. For HDX analysis, an amount of 60 pmol of PPARγ was diluted in D$_2$O according to the scheme in Supporting Information. Samples were incubated for 10 s, 30 s, 1 min, 5 min, and 30 min and performed at least in duplicate. The reaction was quenched by 1:1 dilution into a 0 °C solution of 4 M urea, 200 mM TCEP, with pH adjusted to give a final pH of 2.5. The quenched reaction was immediately injected into a Waters HDX/nanoAcquity system for digestion on an online pepsin column (20 °C, flow rate 125 μL/min) followed by separation on a 10 min RP-HPLC gradient (0.5 °C, flow rate 40 μL/min). The eluent was directed into a Xevo G2 instrument (Waters) with electrospray ionization and lock-mass correction using leu-enkephalin peptide. The online pepsin column used was an Applied Biosystems immobilized pepsin cartridge (2.1 mm × 30 mm). RP-HPLC column used was a Waters C18-BEH, 1.0 mm × 100 mm, with 1.7 μm particles. Electrospray ionization was achieved with a capillary voltage of 3 kV in conjunction with a cone voltage of 75 V and source temperature of 100 °C. Mass calibration was performed with sodium cesium iodide clusters up to *m/z* 2000, giving a mass accuracy of <5 ppm. Two injections of 2 M urea with a pH adjusted to 2.5 were performed between each sample injection to prevent sample carryover. Each sample was analyzed at least in duplicate for each time point. Nondeuterated PPARγ samples were analyzed in the same way for peptide sequencing, using MSe data acquisition and data processing with ProteinLynx Global Server 2.5 software. Uptake of deuterium for each peptide was calculated compared with the nondeuterated control samples using Waters DynamX 3.0.0 software.

Crystallization, Data Collection, and Structure Determination. PPARγ LBD was expressed as N-terminal His-tagged proteins using a pET28 vector and purified as previously described.[35] Crystals of apo-PPARγ were obtained by vapor diffusion at 18 °C using a sitting drop made by mixing 2 μL of protein solution with 2 μL of reservoir solution (0.8 M Na citrate, 0.15 M Tris, pH 8.0). The crystals were soaked for 3 days in a storage solution (1.2 M Na citrate, 0.15 M Tris, pH 8.0) containing the ligand **3a** (0.5 mM). The ligand dissolved in DMSO (50 mM) was diluted in the storage solution so that the final concentration of DMSO was 1%. The storage solution with glycerol 20% (v/v) was used as cryoprotectant. Crystals (0.10 mm × 0.10 mm) of PPARγ/**3a** belong to the space group *C*2 with cell parameters shown in Table 4 of Supporting Information.

X-ray data of the complex PPARγ/**3a** were collected at 100 K under a nitrogen stream using synchrotron radiation (beamline ID30B at ESRF, Grenoble, France). The diffracted intensities were processed using the programs Mosflm[52] and SCALA.[52] Structure solution was performed with AMoRe,[53] using the coordinates of PPARγ/**7j**[15] (PDB code 6QJ5) as the starting model. The coordinates were then refined with CNS[54] and PHENIX[55] including data between 57.84 and 1.95 Å. The statistics of crystallographic data and refinement and the omit map around **3a** are summarized in Table 4 and Figure S19 of Supporting Information.

■ ASSOCIATED CONTENT

ⓢ Supporting Information

The Supporting Information is available free of charge at https://pubs.acs.org/doi/10.1021/acs.jmedchem.0c00048.

Coordinates information for structure representation (PDB)

Experimental protocol for the HDX experiments and HDX figures; X-ray crystal structures of SB1494, SB1495, rosiglitazone, GW9662, LT175, **7j**, **3a** in PPARγ LBD

and double mutant F247C/G346C structure; omit density map around **3a**; SPR sensograms of LT175 and I281A; NMR titration experiments; ELISA phosphorylation assay (PDF)

Conformational dynamics of PPARγ upon LT175 binding (MPG)

Conformational dynamics of PPARγ upon LT175 binding (MPG)

Molecular formula string for **3a** (CSV)

Accession Codes

Coordinates and structure factors of the PPARγ complex with the compound **3a** have been deposited in the Protein Data Bank under the accession code 6T9C. Authors will release the atomic coordinates and experimental data upon article publication.

■ AUTHOR INFORMATION

Corresponding Authors

Roberta Montanari − *Istituto di Cristallografia, Consiglio Nazionale delle Ricerche, 00015 Rome, Italy;* Email: roberta.montanari@ic.cnr.it

Toshimasa Itoh − *Laboratory of Drug Design and Medicinal Chemistry, Showa Pharmaceutical University, Tokyo 194-8543, Japan;* orcid.org/0000-0003-3446-4447; Email: titoh@ac.shoyaku.ac.jp

Giorgio Pochetti − *Istituto di Cristallografia, Consiglio Nazionale delle Ricerche, 00015 Rome, Italy;* orcid.org/0000-0002-3980-3180; Email: giorgio.pochetti@ic.cnr.it

Authors

Davide Capelli − *Istituto di Cristallografia, Consiglio Nazionale delle Ricerche, 00015 Rome, Italy*

Keiko Yamamoto − *Laboratory of Drug Design and Medicinal Chemistry, Showa Pharmaceutical University, Tokyo 194-8543, Japan;* orcid.org/0000-0001-6642-7961

Hirono Awaishima − *Laboratory of Drug Design and Medicinal Chemistry, Showa Pharmaceutical University, Tokyo 194-8543, Japan*

Kimina Nishikata − *Laboratory of Drug Design and Medicinal Chemistry, Showa Pharmaceutical University, Tokyo 194-8543, Japan*

Arjan Barendregt − *Biomolecular Mass Spectrometry and Proteomics, Bijvoet Center for Biomolecular Research and Utrecht Institute for Pharmaceutical Sciences, Science4Life, University of Utrecht, 3584 CH Utrecht, The Netherlands*

Albert J. R. Heck − *Biomolecular Mass Spectrometry and Proteomics, Bijvoet Center for Biomolecular Research and Utrecht Institute for Pharmaceutical Sciences, Science4Life, University of Utrecht, 3584 CH Utrecht, The Netherlands;* orcid.org/0000-0002-2405-4404

Fulvio Loiodice − *Department of Pharmacy & Drug Sciences, University of Bari "Aldo Moro", 70125 Bari, Italy;* orcid.org/0000-0003-3384-574X

Fabio Altieri − *Department of Biochemical Sciences "A. Rossi Fanelli", Sapienza University of Rome, 00185 Rome, Italy*

Alessandro Paiardini − *Department of Biochemical Sciences "A. Rossi Fanelli", Sapienza University of Rome, 00185 Rome, Italy*

Alessandro Grottesi − *CINECA Consorzio Interuniversitario, Sede di Roma, 00185 Rome, Italy*

Luciano Pirone − *Institute of Biostructures and Bioimaging, CNR, 80134 Naples, Italy*

Emilia Pedone − *Institute of Biostructures and Bioimaging, CNR, 80134 Naples, Italy*

Franck Peiretti − *Faculté de Medecine, Aix Marseille Université, INSERM, INRAE, C2VN, 13385 Marseille, France;* orcid.org/0000-0001-7198-0534

Jean Michel Brunel − *Aix Marseille Université, INSERM, SSA, MCT, 13385 Marseille, France;* orcid.org/0000-0002-9355-8980

Complete contact information is available at:
https://pubs.acs.org/10.1021/acs.jmedchem.0c00048

Author Contributions

T.I., R.M., and G.P. designed the research. T.I., E.P., and L.P. performed site-directed mutagenesis. D.C. expressed and purified WT, I281A, and F247C/G346C PPARγ. R.M. and A.P. performed the docking simulation. T.I., H.A., and K.N. performed NMR experiments. K.Y. supervised NMR experiments. A.P. and A.G. performed MD simulations and interpreted the data. R.M. and G.P. designed the HDX experiment. A.B. executed and analyzed the HDX experiment. A.J.R.H. supervised the HDX experiment. R.M. and G.P. performed the *in vitro* kinase assay and the ELISA and phosphoprotein gel stain. F.A. helped in design of ELISA assay and data analysis. F.L. synthesized and provided the ligands. L.P. and E.P. performed the CD experiment on F247C/G346C and WT PPARγ. T.I. performed the CD experiment with GdmCl on I281A and WT PPARγ. J.M.B. and F.P. synthesized **3a**. G.P., D.C., and R.M. performed the X-ray analysis of the complex PPARγ/**3a**. R.M. and G.P. drafted the manuscript. All authors reviewed the final manuscript.

Notes

The authors declare no competing financial interest.

■ ABBREVIATIONS USED

PPAR, peroxisome proliferator-activated receptor; CDK5, cyclin dependent kinase 5; CDK2, cyclin dependent kinase 2; HDX, hydrogen−deuterium exchange; MD, molecular dynamics; T2D, type 2 diabetes; ERK, extracellular signal-regulated kinase; LBD, ligand binding domain; RMSF, root-mean-square fluctuation; PDB, Protein Data Bank; RAR, retinoic acid receptor; TCEP, tris(2-carboxyethyl)phosphine; ELISA, enzyme-linked immunosorbent assay; HSQC, heteronuclear single quantum coherence; SPR, surface plasmon resonance; ED, essential dynamics; WB, washing buffer; DTNB, 5,5-dithiobis[2-nitrobenzoic acid]

■ REFERENCES

(1) Berger, J.; Moller, D. E. The Mechanisms of Action of PPARs. *Annu. Rev. Med.* **2002**, 53, 409−435.

(2) Berger, J. P.; Akiyama, T. E.; Meinke, P. T. PPARs: Therapeutic Targets for Metabolic Disease. *Trends Pharmacol. Sci.* **2005**, 26, 244−251.

(3) Kliewer, S. A.; Sundseth, S. S.; Jones, S. A.; Brown, P. J.; Wisely, G. B.; Koble, C. S.; Devchand, P.; Wahli, W.; Willson, T. M.; Lenhard, J. M.; Lehmann, J. M. Fatty Acids and Eicosanoids Regulate Gene Expression through Direct Interactions with Peroxisome Proliferator-

Activated Receptors Alpha and Gamma. *Proc. Natl. Acad. Sci. U. S. A.* **1997**, *94*, 4318−4323.

(4) Issemann, I.; Green, S. Activation of a Member of the Steroid Hormone Receptor Superfamily by Peroxisome Proliferators. *Nature* **1990**, *347*, 645−650.

(5) Evans, R. M.; Barish, G. D.; Wang, Y. X. PPARs and the Complex Journey to Obesity. *Nat. Med.* **2004**, *10*, 355−361.

(6) Braissant, O.; Foufelle, F.; Scotto, C.; Dauca, M.; Wahli, W. Differential Expression of Peroxisome Proliferator-Activated Receptors (PPARs): Tissue Distribution of PPAR-Alpha,-Beta, and-Gamma in the Adult Rat. *Endocrinology* **1996**, *137*, 354−366.

(7) Forman, B. M.; Chen, J.; Evans, R. M. The Peroxisome Proliferator-Activated Receptors: Ligands and Activators. *Ann. N. Y. Acad. Sci.* **1996**, *804*, 266−275.

(8) Willson, T. M.; Brown, P. J.; Sternbach, D. D.; Henke, B. R. The PPARs: from Orphan Receptors to Drug Discovery. *J. Med. Chem.* **2000**, *43*, 527−550.

(9) Bodmer, M.; Meier, C.; Kraenzlin, M. E.; Meier, C. R. Risk of Fractures with Glitazones: a Critical Review of the Evidence to Date. *Drug Saf.* **2009**, *32*, 539−547.

(10) Nesto, R. W.; Bell, D.; Bonow, R. O.; Fonseca, V.; Grundy, S. M.; Horton, E. S.; Le Winter, M.; Porte, D.; Semenkovich, C. F.; Smith, S.; Young, L. H.; Kahn, R. Thiazolidinedione Use, Fluid Retention, and Congestive Heart Failure: a Consensus Statement from the American Heart Association and American Diabetes Association. *Diabetes Care* **2004**, *27*, 256−263.

(11) Choi, J. H.; Banks, A. S.; Estall, J. L.; Kajimura, S.; Boström, P.; Laznik, D.; Ruas, J. L.; Chalmers, M. J.; Kamenecka, T. M.; Blüher, M.; Griffin, P. R.; Spiegelman, B. M. Anti-Diabetic Drugs Inhibit Obesity-Linked Phosphorylation of PPARgamma by Cdk5. *Nature* **2010**, *466*, 451−456.

(12) Choi, J. H.; Banks, A. S.; Kamenecka, T. M.; Busby, S. A.; Chalmers, M. J.; Kumar, N.; Kuruvilla, D. S.; Shin, Y.; He, Y.; Bruning, J. B.; Marciano, D. P.; Cameron, M. D.; Laznik, D.; Jurczak, M. J.; Schürer, S. C.; Vidović, D.; Shulman, G. I.; Spiegelman, B. M.; Griffin, P. R. Antidiabetic Actions of a Non-Agonist PPARgamma Ligand Blocking Cdk5-Mediated Phosphorylation. *Nature* **2011**, *477*, 477−481.

(13) Banks, A. S.; McAllister, S. E.; Camporez, J. P.; Zushin, P. J.; Jurczak, M. J.; Laznik-Bogoslavski, D.; Shulman, G. I.; Gygi, S. P.; Spiegelman, B. M. An Erk/Cdk5 Axis Controls the Diabetogenic Actions of PPARγ. *Nature* **2015**, *517*, 391−395.

(14) Montanari, R.; Saccoccia, F.; Scotti, E.; Crestani, M.; Godio, C.; Gilardi, F.; Loiodice, F.; Fracchiolla, G.; Laghezza, A.; Tortorella, P.; Lavecchia, A.; Novellino, E.; Mazza, F.; Aschi, M.; Pochetti, G. Crystal Structure of the Peroxisome Proliferator-Activated Receptor Gamma (PPARgamma) Ligand Binding Domain Complexed with a Novel Partial Agonist: a New Region of the Hydrophobic Pocket Could Be Exploited for Drug Design. *J. Med. Chem.* **2008**, *51*, 7768−7776.

(15) Peiretti, F.; Montanari, R.; Capelli, D.; Bonardo, B.; Colson, C.; Amri, E.-Z.; Grimaldi, M.; Balaguer, P.; Pochetti, G.; Brunel, J. M. A Novel N-Substituted Valine Derivative with Unique PPARγ Binding Properties and Biological Activities. *J. Med. Chem.* **2020** (submitted).

(16) Gilardi, F.; Giudici, M.; Mitro, M.; Maschi, O.; Guerrini, U.; Rando, G.; Maggi, A.; Cermenati, G.; Laghezza, A.; Loiodice, F.; Pochetti, G.; Lavecchia, A.; Caruso, D.; De Fabiani, E.; Bamberg, K.; Crestani, M. LT175 is a Novel PPARα/γ Ligand with Potent Insulin-Sensitizing Effects and Reduced Adipogenic Properties. *J. Biol. Chem.* **2014**, *289*, 6908−6920.

(17) Hughes, T. S.; Giri, P. K.; de Vera, I. M. S.; Marciano, D. P.; Kuruvilla, D. S.; Shin, Y.; Blayo, A.-L.; Kamenecka, T. M.; Burris, T. P.; Griffin, P. R.; Kojetin, D. J. An Alternate Binding Site for PPARgamma ligands. *Nat. Commun.* **2014**, *5*, 3571.

(18) Mottin, M.; Souza, P. C.; Skaf, M. S. Molecular Recognition of PPARgamma by Kinase Cdk5/p25: Insights from a Combination of Protein-Protein Docking and Adaptive Biasing Force Simulations. *J. Phys. Chem. B* **2015**, *119*, 8330−8339.

(19) Ribeiro Filho, H. V.; Guerra, J. V.; Cagliari, R.; Batista, F. A. H.; Le Maire, A.; Oliveira, P. S. L.; Figueira, A. C. M. Exploring the Mechanism of PPARγ Phosphorylation Mediated by CDK5. *J. Struct. Biol.* **2019**, *207*, 317−326.

(20) Duarte, M. I.; Pena, D. A.; Nunes Ferraz, F. A.; Berti, D. A.; Paschoal Sobreira, T. J.; Costa-Junior, H. M.; Abdel Baqui, M. M.; Disatnik, M.-H.; Xavier-Neto, J.; Lopes de Oliveira, P. S.; Schechtman, D. Protein Folding Creates Structure-Based, Noncontiguous Consensus Phosphorylation Motifs Recognized by Kinases. *Sci. Signaling* **2014**, *7*, No. ra105.

(21) Brown, N. R.; Noble, M. E.; Endicott, J. A.; Johnson, L. N. The Structural Basis for Specificity of Substrate and Recruitment Peptides for Cyclin-Dependent Kinases. *Nat. Cell Biol.* **1999**, *1*, 438−443.

(22) Tarricone, C.; Dhavan, R.; Peng, J.; Areces, L. B.; Tsai, L. H.; Musacchio, A. Structure and Regulation of the CDK5-p25(nck5a) Complex. *Mol. Cell* **2001**, *8*, 657−669.

(23) Kaufmann, K. W.; Lemmon, G. H.; Deluca, S. L.; Sheehan, J. H.; Meiler, J. Practically Useful: what the Rosetta Protein Modeling Suite Can do for You. *Biochemistry* **2010**, *49*, 2987−2998.

(24) Ruoppolo, M.; Lundstrom-Ljung, J.; Talamo, F.; Pucci, P.; Marino, G. Effect of Glutaredoxin and Protein Disulfide Isomerase on the Glutathione-Dependent Folding of Ribonuclease A. *Biochemistry* **1997**, *36*, 12259−12267.

(25) Nolte, R. T.; Wisely, G. B.; Westin, S.; Cobb, J. E.; Lambert, M. H.; Kurokawa, R.; Rosenfeld, M. G.; Willson, T. M.; Glass, C. K.; Milburn, M. V. Ligand Binding and Co-Activator Assembly of the Peroxisome Proliferator-Activated Receptor-Gamma. *Nature* **1998**, *395*, 137−143.

(26) Chrisman, I. M.; Mou, T. C.; Sprang, S. R.; Hughes, T. S. PPARgamma LBD Complexed with GW1929 (PDB 6D8X). To be published.

(27) Hughes, T. S.; Chalmers, M. J.; Novick, S.; Kuruvilla, D. S.; Chang, M. R.; Kamenecka, T. M.; Rance, M.; Johnson, B. A.; Burris, T. P.; Griffin, P. R.; Kojetin, D. J. Ligand and Receptor Dynamics Contribute to the Mechanism of Graded PPARgamma Agonism. *Structure* **2012**, *20*, 139−150.

(28) Hamuro, Y.; Coales, S. J.; Morrow, J. A.; Molnar, K. S.; Tuske, S. J.; Southern, M. R.; Griffin, P. R. Hydrogen/Deuterium-Exchange (H/D-Ex) of PPARgamma LBD in the Presence of Various Modulators. *Protein Sci.* **2006**, *15*, 1883−1892.

(29) Bae, H.; Jang, J. Y.; Choi, S.-S.; Lee, J.-J.; Kim, H.; Jo, A.; Lee, K.-J.; Choi, J.-H.; Suh, S. W.; Park, S. B. Mechanistic Elucidation Guided by Covalent Inhibitors for the Development of Anti-Diabetic PPARγ Ligands. *Chem. Sci.* **2016**, *7*, 5523−5529.

(30) Brust, R.; Lin, H.; Fuhrmann, J.; Asteian, A.; Kamenecka, T. M.; Kojetin, D. J. Modification of the Orthosteric PPARgamma Covalent Antagonist Scaffold Yealds an Improved Dual-Site Allosteric Inhibitor. *ACS Chem. Biol.* **2017**, *12*, 969−978.

(31) Hughes, T. S.; Shang, J.; Brust, R.; de Vera, I. M. S.; Fuhrmann, J.; Ruiz, C.; Cameron, M. D.; Kamenecka, T. M.; Kojetin, D. J. Probing the Complex Binding Modes of the PPARgamma Partial Agonist 2-chloro-N-(3-chloro-4-((5-chlorobenzo[d]thiazol-2-yl)thio)phenyl)-4-(trifluoromethyl)benzenesulfonamide (T2384) to Orthosteric and Allosteric Sites with NMR Spectroscopy. *J. Med. Chem.* **2016**, *59*, 10335−10341.

(32) Jang, J. Y.; Koh, M.; Bae, H.; An, D. R.; Im, H. N.; Kim, H. S.; Yoon, J. Y.; Yoon, H.-J.; Han, B. W.; Park, S. B.; Suh, S. W. Structural Basis for Differential Activities of Enantiomeric PPARgamma Agonists: Binding of S35 to the Alternate Site. *Biochim. Biophys. Acta, Proteins Proteomics* **2017**, *1865*, 674−681.

(33) Laghezza, A.; Piemontese, L.; Cerchia, C.; Montanari, R.; Capelli, D.; Giudici, M.; Crestani, M.; Tortorella, P.; Peiretti, F.; Pochetti, G.; Lavecchia, A.; Loiodice, F. Identification of the First PPARalpha/gamma Dual Agonist Able to Bind to Canonical and Alternative Sites of PPARgamma and to Inhibit its Cdk5-mediated Phosphorylation. *J. Med. Chem.* **2018**, *61*, 8282−8298.

(34) Pochetti, G.; Godio, C.; Mitro, N.; Caruso, D.; Galmozzi, A.; Scurati, F.; Loiodice, F.; Fracchiolla, G.; Tortorella, P.; Laghezza, A.; Lavecchia, A.; Novellino, E.; Mazza, F.; Crestani, M. Insights into the Mechanism of Partial Agonism: Crystal Structures of the Peroxisome Proliferator-Activated Receptor Gamma Ligand-Binding Domain in

the Complex with two Enantiomeric Ligands. *J. Biol. Chem.* **2007**, *282*, 17314−17324.

(35) Fracchiolla, G.; Laghezza, A.; Piemontese, L.; Tortorella, P.; Mazza, F.; Montanari, R.; Pochetti, G.; Lavecchia, A.; Novellino, E.; Pierno, S.; Conte Camerino, D.; Loiodice, F. New 2-aryloxy-3-phenyl-propanoic acids as Peroxisome Proliferator-Activated Receptors Alpha/Gamma Dual Agonists with Improved Potency and Reduced Adverse Effects on Skeletal Muscle Function. *J. Med. Chem.* **2009**, *52*, 6382−6393.

(36) Pochetti, G.; Mitro, N.; Lavecchia, A.; Gilardi, F.; Besker, N.; Scotti, E.; Aschi, M.; Re, N.; Fracchiolla, G.; Laghezza, A.; Tortorella, P.; Montanari, R.; Novellino, E.; Mazza, F.; Crestani, M.; Loiodice, F. Structural Insight into Peroxisome Proliferator-Activated Receptor Gamma Binding of two Ureidofibrate-Like Enantiomers by Molecular Dynamics, Cofactor Interaction Analysis, and Site-Directed Muta-genesis. *J. Med. Chem.* **2010**, *53*, 4354−4366.

(37) Porcelli, L.; Gilardi, F.; Laghezza, A.; Piemontese, L.; Mitro, N.; Azzariti, A.; Altieri, F.; Cervoni, L.; Fracchiolla, G.; Giudici, M.; Guerrini, U.; Lavecchia, A.; Montanari, R.; Di Giovanni, C.; Paradiso, A.; Pochetti, G.; Simone, G. M.; Tortorella, P.; Crestani, M.; Loiodice, F. Synthesis, Characterization and Biological Evaluation of Ureidofi-brate-Like Derivatives Endowed with Peroxisome Proliferator-Activated Receptor Activity. *J. Med. Chem.* **2012**, *55*, 37−54.

(38) Fracchiolla, G.; Laghezza, A.; Piemontese, L.; Parente, M.; Lavecchia, A.; Pochetti, G.; Montanari, R.; Di Giovanni, C.; Carbonara, G.; Tortorella, P.; Novellino, E.; Loiodice, F. Synthesis, Biological Evaluation and Molecular Investigation of Fluorinated Peroxisome Proliferator-Activated Receptors alpha/gamma Dual Agonists. *Bioorg. Med. Chem.* **2012**, *20*, 2141−2151.

(39) Laghezza, A.; Pochetti, G.; Lavecchia, A.; Fracchiolla, G.; Faliti, S.; Piemontese, L.; Di Giovanni, C.; Iacobazzi, V.; Infantino, V.; Montanari, R.; Capelli, D.; Tortorella, P.; Loiodice, F. New 2-(aryloxy)-3-phenylpropanoic Acids as Peroxisome Proliferator-Acti-vated Receptor alpha/gamma Dual Agonists Able to Upregulate Mitochondrial Carnitine Shuttle System Gene Expression. *J. Med. Chem.* **2013**, *56*, 60−72.

(40) Bourguet, W.; Vivat, V.; Wurtz, J. M.; Chambon, P.; Gronemeyer, H.; Moras, D. Crystal Structure of a Heterodimeric Complex of RAR and RXR Ligand-Binding Domains. *Mol. Cell* **2000**, *5*, 289−298.

(41) Bruning, J. B.; Chalmers, M. J.; Prasad, S.; Busby, S. A.; Kamenecka, T. M.; He, Y.; Nettles, K. W.; Griffin, P. R. Crystal Structure of PPARgamma Bound to Partial Agonist nTZDpa. *Structure* **2007**, *15*, 1258−1271.

(42) Jang, J. Y.; Kim, H.; Kim, H.-J.; Suh, S. W.; Park, S. B.; Han, B. W. Structural Basis for the Inhibitory Effects of a Novel Reversible Covalent Ligand on PPARγ Phosphorylation. *Sci. Rep.* **2019**, *9*, 11168.

(43) Li, P.; Fan, W.; Xu, J.; Lu, M.; Yamamoto, H.; Auwerx, J.; Sears, D. D.; Talukdar, S.; Oh, D.; Chen, A.; Bandyopadhyay, G.; Scadeng, M.; Ofrecio, J. M.; Nalbandian, S.; Olefsky, J. M. Adipocyte NCoR Knockout Decreases PPARγ Phosphorylation and Enhances PPARγ Activity and Insulin Sensitivity. *Cell* **2011**, *147*, 815−826.

(44) Lu, J.; Chen, M.; Stanley, S. E.; Li, E. Effect of Heterodimer Partner RXRalpha on PPARgamma Activation Function-2 Helix in Solution. *Biochem. Biophys. Res. Commun.* **2008**, *365*, 42−46.

(45) Combs, S. A.; Deluca, S. L.; Deluca, S. H.; Lemmon, G. H.; Nannemann, D. P.; Nguyen, E. D.; Willis, J. R.; Sheehan, J. H.; Meiler, J. Small-Molecule Ligand Docking into Comparative Models with Rosetta. *Nat. Protoc.* **2013**, *8*, 1277−1298.

(46) *The PyMOL Molecular Graphics System*, version 2.0; Schroedinger, LLC..

(47) *Molecular Operating Environment (MOE)*, version 2013.08; Chemical Computing Group ULC (1010 Sherbooke St. West, Suite No. 910, Montreal, QC, Canada, H3A 2R7), 2018.

(48) Bussi, G.; Donadio, D.; Parrinello, M. Canonical Sampling through Velocity Rescaling. *J. Chem. Phys.* **2007**, *126*, 014101.

(49) Di Pierro, M.; Elber, R.; Leimkuhler, B. A Stochastic Algorithm for the Isobaric-Isothermal Ensemble with Ewald Summations for all Long Range Forces. *J. Chem. Theory Comput.* **2015**, *11*, 5624−5637.

(50) Chen, A. A.; Pappu, R. V. Parameters of Monovalent Ions in the AMBER-99 Forcefield: Assessment of Inaccuracies and Proposed Improvements. *J. Phys. Chem. B* **2007**, *111*, 11884−11887.

(51) Amadei, A.; Linssen, A. B. M.; Berendsen, H. J. C. Essential Dynamics of Proteins. *Proteins: Struct., Funct., Genet.* **1993**, *17*, 412−425.

(52) Leslie, A. G. W. Joint CCP4 and ESFEACMB Newslwtter on Protein. *Protein Crystallogr.* **1992**, *26*, 27−33.

(53) Navaza, J. *Acta Crystallogr., Sect. A: Found. Crystallogr.* **1994**, *50*, 157−163.

(54) Brunger, A. T.; Adams, P. D.; Clore, G. M.; DeLano, W. L.; Gros, P.; Grosse-Kunstleve, R. W.; Jiang, J. S.; Kuszewski, J.; Nilges, M.; Pannu, N. S.; Read, R. J.; Rice, L. M.; Simonson, T.; Warren, G. L. Crystallography & NMR System: A New Software Suite for Macromolecular Structure Determination. *Acta Crystallogr., Sect. D: Biol. Crystallogr.* **1998**, *54* (Part 5), 905−921.

(55) Adams, P. D.; Afonine, P. V.; Bunkoczi, G.; Chen, V. B.; Davis, I. W.; Echols, N.; Headd, J. J.; Hung, L.-W.; Kapral, G. J.; Grosse-Kunstleve, R. W.; McCoy, A. J.; Moriarty, N. W.; Oeffner, R.; Read, R. J.; Richardson, D. C.; Richardson, J. S.; Terwilliger, T. C.; Zwart, P. H. *Acta Crystallogr., Sect. D: Biol. Crystallogr.* **2010**, *66*, 213−221.